ARTICLE

Defect-Induced Blue and Black TiO_2: Inspiring Next Generation Photocatalysts for Solar Hydrogen Production†

Received 00th January 20xx,
Accepted 00th January 20xx

DOI: 10.1039/x0xx00000x

Sanjeev Gupta,[a] Katherine Armstrong,[b] Emma Richards,[b] Andrea folli,[b] Miki Hasegawa,[c] Shinya Hayami,[d,e] Haresh Manyar,[f] Balasubramanian Viswanathan[a] and Parasuraman Selvam*[a,e,f,g]

Generating hydrogen *via* photocatalysis using artificial or natural light remains a significant challenge due to insufficient energy conversion in the visible-light spectrum. Recent efforts have focused on synthesizing defect-enriched photocatalysts, with titania (TiO_2) being one of the most extensively studied and modified materials. This study employs both physical and chemical methods to fine-tune intrinsic defects, such as trapped electrons, oxygen vacancies, and/or Ti^{3+} centers, at the surface, subsurface, or within the bulk crystal lattice. We report the synthesis of blue titania, achieved through a single-step hydrogen reduction process at 20 bar pressure and 450°C using commercial white titania, which resulted in a 2.6-fold enhancement in solar hydrogen evolution. This performance was compared with chemically reduced, defect-enriched, colored crystalline TiO_2, prepared under ambient conditions using $NaBH_4$ as a reductant in either a hydrogen or argon atmosphere.

1. Introduction

Over the past couple of decades, enormous efforts have been spent to design materials that efficiently store solar energy into chemical bonds for later utilisation, a process now commonly referred to as solar fuels generation. Titanium dioxide has been one of the most studied materials for this purpose, since its first use as a photoanode in the Fujishima-Honda cell.[1] The study of defect chemistry in TiO_2 is of particular importance as intrinsic defects and extrinsic defects, such as dopants, play a critical role on properties such as light absorption, electronic conductivity, energy band gap, etc.[1-3] As such, from the 1980's onwards, TiO_2 doping strategies, including p-block elements doping (C, N and S etc.),[4-7] transition metal ions doping,[8] as well as metal-metal,[9] metal-nonmetal[10,11] and nonmetal-nonmetal codoping,[12] have been primarily employed to improve solar light harvesting in TiO_2-sensitised photoreactions (or photocatalytic reactions), including the ones for solar fuels (mostly H_2) production. Furthermore, to improvise more, Intensive research efforts are going underlying for physical and chemical processes by tailored band position in order to improve the electronic properties as well as the photocatalytic activity.

The discovery by Chen *et al*.[13] in 2011, that hydrogenated TiO_2 nanocrystals (black) with an extended degree of surface disorder exhibited strong absorbance of visible light and efficient generation of hydrogen through direct photocatalytic water splitting, thus paved the way to engineer bulk and surface defects via reduction and that they provide trapping sites for charge carriers and hence slow the recombination of photoexcitons. Tominaka *et al*.[14,15] reported reduced titania using CaH_2 and $NaBH_4$ as reducing agent inspired by Hayward *et al*.[16] who demonstrated first-time low temperature reduction using metal hydride. Naldoni *et al*.[17] reported on reducing the white crystalline Evonik P25 under H_2 atmosphere will form pale blue colour powder with unmodified absorption spectra. Kalathil *et al*.[18] reported band gap narrowing of Evonik P25 using an electrochemically biofilm in a solution of acetate as hole scavenger. Lu *et al*.[19] reported black P25 at room temperature (15°C) under 35 bar pressure keeping for 20 days. Tan *et al*.[20] reported large-scale production of coloured titania through a controllable solid-state reaction between $NaBH_4$ and TiO_2 (Evonik P25) in Ar environment. However, it did not mention any sodium-ion incorporation inside the TiO_2 lattice Ye *et al*.[21] reported black titania nanoparticles by Mg reduction of Evonik P25. In addition to these reports, other methods [22-24] to produce black and blue titania have also been proposed, often correlated by computational work in order to understand the nature of the defects and the overall structure of final material.

However, one of the significant challenges in the design of highly defective (blue or black) titania remains the control of the concentration of defects such as trapped electrons/Ti^{3+}

a. National Centre for Catalysis Research and Department of Chemistry, Indian Institute of Technology-Madras, Chennai, India. Tel: +91-44-2257-4235; E-mail: selvam@iitm.ac.in
b. School of Chemistry, Cardiff University, Cardiff CF10 3AT, United Kingdom
c. Department of Chemistry and Biological Science, College of Science and Engineering, Aoyama Gakuin University, 252-5258 Kanagawa, Japan
d. Department of Chemistry, Faculty of Advanced Science and Technology, Kumamoto University, Kumamoto 860-8555, Japan
e. International Research Organization for Advanced Science and Technology, Kumamoto University, Kumamoto 860-8555, Japan
f. School of Chemistry and Chemical Engineering, Queen's University Belfast, David-Keir Building, 39-123, Stranmillis Road, Belfast BT9 5AG, United Kingdom
g. Department of Chemical Engineering and Biotechnology, University of Cambridge, Philippa Fawcett Drive, Cambridge CB3 0AS, United Kingdom

†Electronic Supplementary Information (ESI) available: [Powder XRD patterns, Rietveld-refined XRD patterns, DRSUV absorbance spectra, HR-TEM, Nitrogen adsorption-desorption isotherms and Raman spectra]. See DOI: 10.1039/x0xx00000x

(surface/subsurface vs bulk, lattice vs interstitial), oxygen and titanium vacancies, during synthesis. Furthermore, what remains even more elusive is a fundamental structure-activity understanding of highly defective TiO_2 photocatalysts; especially considering that extensive experimental evidence suggests that a high concentration of defects leads to magnéli phase, which is deleterious for photocatalytic activity. Therefore, in this study, we have carefully prepared coloured titania using two different strategies, viz., physical and chemical methods. The former employs a single-step reduction in the H_2 atmosphere under controlled pressure and temperature, while in the latter case, a solid-state reaction is employed using $NaBH_4$ in H_2 and Ar atmosphere. The resulting samples were used to study the photocatalytic hydrogen evolution. A preliminary account of the work is presented elsewhere.[25-29].

2. Experimental Section

2.1. Starting Materials

AEROXIDE® TiO_2 P25, a hydrophilic fumed titanium dioxide fine white powder with a high specific surface area, was purchased from the Evonik industry, Sodium borohydride ($NaBH_4$; Merck, ≥ 95%), Ethanol (C_2H_5OH; Changshu Hongsheng Fine Chemicals Ltd. > 99.9%), Carbinol (CH_3OH; Sisco Research Laboratory Ltd. > 99.8%). All chemicals were used as received without further purification.

2.2. Synthesis of coloured titania

A series of coloured titania were prepared both by physical and chemical methods (Figure 1) using the typical white coloured P25-WT. Blue hydrogenated TiO_2 (P25-PBL) was prepared by taking 250 mg of aeroxide P25-WT in a 300 mL capacity Parr Autoclave. The autoclave was purged for 20 minutes through Ultra high pure (UHP) H_2 to remove other gases. Further, the autoclave was kept at 20.0 bar in UHP H_2 at a temperature of 450°C for 24 h. Initially slow heating rate maintained up upto (1°C/min) till 175°C, then increased ramp rate was by (5°C/min) further, after 24 h cooled, it rapidly overnight.

In another synthesis, 3 g P25-WT is mixed with 2 g of $NaBH_4$ and ground it manually for nearly 15 minutes. Then the mixture was transferred in a quartz boat and well placed into a tubular furnace, and heated (@10°C/min) in a H_2 flow for 10 minutes in a range 300-415°C. After natural cooling down to room temperature obtained mixture was further washed several times with distilled water and ethanol to remove unreacted $NaBH_4$ further dry at 70°C in a hot air oven for 24 h to obtain series of coloured titania designed as (P25-CLB, P25-CBL, P25-CBB and P25-CBK). In another set, 2g P-25 is mixed with 800 mg of $NaBH_4$ and ground manually for nearly 15 minutes. Then the mixture was transferred in a quartz boat and well placed into a tubular furnace, and heated in a under Ar flow for 1 h at 330-380°C (@10°C/min) to obtain (P25-CBL(A)) and (P25-CBB(A)).

2.3 Characterisation

Titania samples were systematically characterised by various spectroscopic techniques viz., Powder X-ray diffraction (XRD) patterns of the TiO_2 samples were recorded from an X-Ray diffractometer (Bruker D8 Advance) using Cu Kα (0.15406 nm) in 2θ range of (10°-80°). Material Analysis Using Diffraction (MAUD) software is being used for structural parameter refinement. Transmission electron microscopy (TEM) analysis performed on JEOL USA JEM 2100 LaB6 (200 kV), TEM samples were finely ground using an agate mortar and then dispersed in ethanol, sonicate it for 30 min. A drop of the suspension was gently deposited on holy carbon film supported on a copper 200 mesh grid. The specimens after solvent evaporation were inserted in a column of TEM. TEM micrograph were recorded for wide region in order to provide a truly representative and statistical map of TiO2 powders other sample was done at High-resolution PC controlled 200 kV TEM. Nitrogen sorption isotherms were measured at 77 K using Micrometrics ASAP 2020 surface area analyser, in which catalysts were outgassed at 473 K for 4h before the measurements. Helium was used as the carrier gas. Specific surface area was calculated using BET (Brunauer-Emmett-Teller) equation, and pore-size distribution were obtained from the desorption branch of the isotherm by the BJH (Barrett-Joyner-Halenda) method.

Diffuse reflectance ultra-violet visible (DRUV-VIS) spectroscopy measurements were performed in Jasco V-650 spectrophotometer in a range 200-800 nm using $BaSO_4$ as reflectance sample and Kubelka-Munk (K-M) formalism was used for onset band-gap determination. Photoluminescence and excitation spectra were recorded on spectrophotometer Fluorolog 3-22 (Horiba Jobin Yvon). The excitation wavelength used is 350 nm. The absolute quantum yield was calculated using the apparatus (Hamamatsu 9920-02). Electron paramagnetic resonance (EPR) spectra at X band frequencies were recorded at 77 K on a Bruker EMX spectrometer equipped with a Bruker ER-4122-SHQE resonator or on a JEOL Model JES FA200 spectrometer equipped with a cylindrical type (TE_{011} cylindrical) resonator and provide better modulation uniformity. Spectra were recorded at 100 kHz field modulation frequency, 0.1 mT field modulation amplitude, 5.12 ms time constant, 10.24 ms conversion time, and resolution of the magnetic induction sweep of at least 4096 points. Raman measurement were performed on MultiRAM FT-Raman spectrometer uses a 1W Nd:YAG air cooled laser to deliver a wavelength of 522-625 nm for excitation with a resolution range of 4 - 15 cm^{-1} recorded at the intensity of 10 mW. The spectra were recorded at room temperature for all samples.

X-ray photoelectron spectral (XPS) measurements were performed with an Omicron Nanotechnology spectrometer with the hemispherical analyser. The monochromatic Mg Kα X-source (E = 1253.6 eV) was operated at 15 kV and 20 mA. Survey scans were performed with pass energy of 50 eV and a scan width of 0.5 eV. For the narrow scans, the analyser pass energy of 20 eV was applied with a scan rate of 0.1 eV per sec. The base pressure in the analysis chamber is 1 x 10^{-9} Torr. Approximately 50 mg of the sample is taken and then made into a pellet by applying 15 bar pressure. This was then loaded onto a stainless steel plate with the help of carbon tape and transferred to the sample chamber, and then a vacuum of 8 x 10^{-7} Torr was applied for 18 h and then the sample was transferred to the analysis chamber. The spectra were deconvoluted using CasaXPS

software. All the ranges are corrected to carbon binding energy at 284.7 eV. AE spectra were recorded using Thermo scientific K–Alpha X-Ray spectrophotometer (X-Ray Source: Al K–Alpha, Energy-1486.6 eV). The spectra were recorded in integral mode using constant analyser mode (CAM) the number of scans were performed at 100 eV. The obtained spectra were differentiated using CasaXPS software. Surface composition and concentrations were calculated from relative appropriate area under signal.

Photo-electrochemical experiments were recorded in a conventional three-electrode set-up using VersaSTAT 4. Here, Pt foil used as a counter electrode, Ag/AgCl as a reference electrode. Then, the potential was converted into NHE potential scale. The working electrode was prepared by (1 mg) active material casting on (1 × 1) cm^2 exposed aluminium foil. The material ink consists of 1 mL water, 1 mL isopropanol, 10 µL Nafion®. Millipore water (18 MΩ) was used in all photo-electrochemical experiments. Electrochemical impedance spectroscopy (EIS) was measured between 100 kHz to 100 mHz with 10 mV rms amplitude in an open circuit potential. The EIS was recorded in the presence of xenon lamp (280 W) in 0.5 M H_2SO_4.

Photocatalytic hydrogen evolution was performed on various prepared coloured titania and commercial titania using a light source as a solar simulator (Model-SS50AAA) of photo emission tech., Inc. (150 W). The aqueous solution of water and methanol (3:1) was taken in two mouths jacketed closed double-layer glass reactor having a capacity of 315 mL also fitted with a gas purging set-up and attached quartz plate on top since it is a vertical set-up. The amount of 30 mg catalyst was added to the solution. Now the closed glass reactor, under constant stirring, was purged with high-purity nitrogen gas before the start of the experiment until no oxygen was left in the reactor vacant space. Further to check whether the complete oxygen was removed from the closed glass vessel. Gas Chromatography (GC) measurements were performed on Perkin Elmer Clarus 580 model GC using the column Molecular sieves–13X attached with thermal conductivity detector (TCD). The nitrogen is used at 80 psi pressure as a carrier gas to detect hydrogen gas. The calibration was done by injecting the set of volumes (mL) of standard high-purity hydrogen gas and oxygen gas to get the relative peak area in the chromatograph. Further 0.2 mL evolved gas under irradiation was ejected with the help of a gas syringe manually from the glass reactor mouth jacket closed with silicon rubber septa during the reaction under solar irradiation at a specific time-to-time interval. The unknown gas used for detection, the relative peak area of unknown gas w.r.t to standard sample of known concentration will detect the amount of evolved hydrogen gas.

3. Results and Discussion

3.1 Structural studies

Powder XRD patterns of white (Figure 2a) and blue (Figure 2b) titania samples prepared *via* physical method show characteristic reflections typical of both anatase and rutile phases. Further, the structural refinement values obtained by Rietveld method (Figure 2c and 1d) and the computed structural paramerters and phase composition values are listed in Table 1. It can be senn from this table that the lattice constant and the phase composition values are in excellent agreement with the reported values.[30,31] Furhter, it can also be noticed from Figure 2 that there is an apparent increase in the intensity of the rutile phase for the blue titania which is expected due to conversion of anatase to rutile at elevated temperature. The Scherrer formula given in equation (1) is typically used for estimating the crystallite size of nanomaterials. Further, it is clear from this equation that the line-broadending at half the maximum intensity correlation well with the size of sub-micrometre or nanometre crystallites with the size, i.e., smaller the crystallites larger the line-broadening.

$$\tau = \frac{\kappa \lambda}{\beta \cos\theta} \qquad (1)$$

where τ is the crystallite size (in Å), κ is a constant related to crystallite shape and has a typical value of 0.89 but varies with the actual shape of the crystallite, λ is the X-ray wavelength (in Å), β is the full-width at the half-maximum (FWHM) height of the reflection in radians, and θ is the Bragg angle (in °) of the reflection.

we observed an increase in crystallite size and as expected, an increase in rutile phase (%) (P25-PBL). In Figure 3, the Rietveld refined XRD patterns depict the reflections characteristic of anatase and rutile phase for all coloured titania materials prepared *via* the chemical method under hydrogen atmosphere. In addition that the appearance of several new reflections (2θ) was clearly observed in P25-CBB and P25-CBK (18.9°, 31.4° and 42.5°), which indicate and suggests that new crystalline phases may have been formed during chemical reduction treatment. These phases are mainly a mixture of several reduced titanium oxides like Ti_4O_7, Ti_9O_{10}, Ti_9O_{17}, etc. We also clearly observed peak broadening in coloured samples. It might be due to an increase in surface disorder and breaking of symmetry Ti-O-Ti tangling bonds. Therefore, as a result, disorder-induced lattice strains and reduced crystallite size and values are tabulated in Table 2. Further, Raman spectroscopy measurements have been performed, which clearly support XRD results. Furthermore, XRD patterns in (Figure S3, ESI†) show the coloured titania materials prepared *via* the chemical method under Ar atmosphere designated as P25-CBL(A) and P25-CBB(A). The Rietveld refined XRD pattern in (Figure S4, ESI†) clearly suggests it has similar characteristics and reflections features which we observed in coloured titania materials prepared *via* the chemical reduction method under a hydrogen atmosphere. The refined structural parameters were calculated and tabulated in Table 3.

3.2 Optical band gap measurements

Diffuse reflectance UV-Visible absorbance spectra (DRSUVS) were recorded for all the prepared coloured titania materials to study the optical response (Figure 4 (a) and (c)). It was clearly observed that extent of light absorption from UV to UV-visible region for each prepared (blue to black) coloured titania

materials. The observation is well agreement with literature.[13,20,32] In a prepared P25-PBL a band narrowing with a clear shift relative to P25-WT was observed (Figure 4 (a) and (b)), whereas coloured titania prepared through metal hydride reduction in H_2 (Figure 4 (c) and (d)) and Ar atmosphere (Figure S5 (a) and (b), ESI†), a tailored broadband appeared and showed higher and higher absorbance as blue to black colour appears in titania. It suggests it almost covered the visible region as the colour became darker, from (blue to black). The spectral data were also analysed by using a modified Kubelka-Munk (K-M) function w.r.t band gap energy (eV) using the tauc method.[33-35] An attempt has been made to calculate the onset band gap where the intercept on the X-axis of the extrapolated linear part of the plots at $[F(R).hv]^{½}$ = 0 used for all prepared and commercial titania materials under investigation as shown in (Figure 4 (b) and (d))**.** The energy band gap values are listed in Table 1, 2 and 3. At this juncture, we did not observe any significant change for onset band gap by following the Tauc method to calculate the onset band gap in coloured titania prepared via the chemical reduction method it is still an underlying challenge to calculate the appropriate energy band gap for those spectra in which tailored and broad absorption occurs, although onset (E_g) for P25-WT is 3.21 eV, which is excellent with reported data. Therefore, it's still challenging and difficult to comment on overall how much exact alteration happened in an energy band gap for prepared coloured titania materials.

3.3 Morphological studies

Figure 5(a) depicts the TEM micrograph of commercial P25-WT, which exhibits fine-particle morphology. It consists of individual crystallites of an average dimension of about 25 nm can clearly be seen from particle size distribution (inset) in Figure 4(a), which is in line with crystallite size in (Table 1) calculated by XRD using the Scherrer equation.[36] Figure 5(b) shows TEM micrograph of P25-PBL, no significant change observed in any morphology for P25-PBL relative to P25-WT. Although, as expected, an increase in average particle size for P25-PBL was observed as compared to P25-WT. The average particle size distribution (inset) in Figure 4(b) increased is about 45 nm, suggesting slight anatase to rutile phase transformation at high temperature and pressure, which was well in agreement with our XRD results. On the other side, the TEM images for coloured titania prepared via chemical method under hydrogen atmosphere in (Fig S6, ESI†) suggests the surface gets disordered or disintegrated and it get more increases as colour becomes more intense (blue to black) from P25-CBB to P25-CBK relative to commercial titania P25-WT the crystallite size was calculate from XRD and observed values were tabulated in Table 2. It was observed the coloured titania prepared via the chemical reduction method has less crystallite size compared with P25-WT. Finally, it can be seen from TEM images that the material consists of individual crystallites of average dimension of ~ 22 *nm*, which is in line with the computed crystallite size (Table 2) using XRD.

3.4. Surface area and porosity

The textural properties were evaluated and the nitrogen sorption isotherms with their respective pore size distributions (inset) are presented in (Figure S7, S8 and S9, ESI†) which show a typical type III isotherm[37,] and values were tabulated in Table (1, 2 and 3). It was observed and well expected (Figure S7, ESI†) that there will be a significant decrease in specific surface area for material P25-PBL relative to P25-WT. The observed crystallite size for anatase and rutile phases in P25-PBL was increased relative to P25-WT, it was well in agreement with the increase in average particle size observed in our TEM results. In general, the crystallites are much larger in the rutile phase so mostly lower specific surface area. Whereas coloured titania samples were prepared *via* the chemical reduction method in (Figure S8 and S9, ESI†), no significant changes were observed except for P25-CBK. In black coloured P25-CBK a significant decrease in the crystallite size was observed for both anatase and rutile phases. It is attributed due to increased surface -Ti-O-Ti- disorderliness and amorphous nature. It also impacts specific surface area; as expected, it gets slightly increased for materials prepared both in H_2 and Ar atmosphere.

3.5. Electron paramagnetic resonance studies

Continuous wave (CW) electron paramagnetic resonance (CW-EPR) spectroscopy was conducted to identify the nature of the crystal defects associated with the reduction of P25 TiO_2 as well as probing their photochemical behaviour. EPR spectra recorded before and after in-situ UV light irradiation are reported in Figure 6 for P25-CBL(A) and P25-CBB(A) respectively, i.e., the blue and blue-black TiO_2 samples obtained via chemical reduction under Ar atmosphere. Spectra simulations for P25-CBL(A) revealed anisotropic **g** tensors with principal values reported in Table 4. Before UV irradiation, the signal at *g* values > 2 exhibit an anisotropic **g** tensor (A in Table 4) that could be attributed to a vacancy defect,[38] a signal often found in TiO_2 nanoparticle. At *g* values < 2, at least two signals are superimposed (B and C in Table 4) and characterised by an anisotropic **g** tensor with axial symmetry. These tensors could be assigned to surface Ti^{3+} in anatase and rutile phases. Surface Ti^{3+} species do normally exhibit broader EPR lines than bulk or interstitial Ti^{3+} species.[38] In this case, the very high concentration of chemically generated reduced centres (i.e. Ti^{3+}) at the surface of the nanoparticles significantly contributes to the line broadening due to extensive spin exchange and dipolar interactions (both of which are expected to broaden EPR lines linearly with concentration).

Upon UV irradiation, two new signals (D and E in Table 4) appear at *g* values > 2 according to simulations. Both **g** tensors can be ascribed to paramagnetic hole centres (following excitation of valence band electrons to conduction band) in different crystallographic environments, one matching values reported for Ti^{4+}–$O^{\bullet-}$–Ti^{4+}–OH^- in anatase; whilst the second one is similar to what reported for a Ti^{4+}–O_2^- in anatase.[37]

To our best understanding, the EPR signal of P25-CBB(A) is characterised by very similar paramagnetic species as P25-CBL(A). However, the even greater concentration of surface reduced Ti^{3+} (induced by the more extensive reduction of the starting material) broadens the spectrum beyond the resolution of the different paramagnetic species, complicating any attempts at spectral simulation. Although not as evident as in

the case of P25-CBL(A), a small vacancy defect is visible in the bottom spectrum of Figure 7 and upon UV irradiation an increase of the signals associated with hole centres is appreciable. Furthermore, a new signal (indicated by the arrow in Figure 7) appears in the case of irradiated P25-CBB(A). This matches what was reported for the perpendicular component of the axial g tensor of interstitial Ti^{3+} (the parallel component of the tensor is concealed by the intense broad signal arising from surface Ti^{3+}).[39] Increase in defects concentration is in perfect agreement with UV-vis data. The colour, from white to blue to black, can be reconciled to an increasingly more amorphous surface characterised by an increasingly higher concentration of reduced species/crystal defects induced by the chemical reduction of the solid material[13,] which broadens the optical absorption of the material up to across the entire visible light portion of the electromagnetic spectrum, in the case of the black sample. The samples obtained via hydride reduction under H_2 atmosphere (Figure 7) exhibited the same type of crystal defects as the ones obtained under an inert Ar atmosphere, with identical EPR spectral broadening from blue to black specimens due to increased concentrations of crystal defects as previously described.

Interestingly, the situation is remarkably different in the case of the P25 sample hydrogenated under high H_2 pressure (Figure 8), i.e., P25-PBL. The EPR spectra for this sample do not show any evidence of trapped holes in the form of $O^{\bullet-}$, or trapped electrons in the form of Ti^{3+}. On the contrary, a narrow (8-9 MHz linewidth) line occurs at $g = g_e$ that can be safely attributed to an F-centre,[40] i.e., an oxygen vacancy containing a single electron, which formation is induced by the treatment with hydrogen at ultra-high pressure and high temperature. It is believed that the colour of this differently treated sample is predominantly due to the occurrence of this specific colour centre.

3.6. Photoluminescence studies

Photoluminescence spectra can be used to understand the rate of excitons in a semiconductor since emissions results from the recombination of charge carriers.[41-44] Here, Figure 9 we clearly observed that all prepared coloured titania shows less weak signal relative to aeroxide P25-WT which suggests us coloured titania have slow recombination of charge carriers and help to facilitates charge transfers to surface. The peaks observed in a region 440-550 nm is basically due to crystals defects and oxygen vacancy. Further, the absolute luminescence quantum yields were calculated for commercial titania P25-WT (QY - 0.5%) and P25-CBL (QY - 0.6%) but the values for P25-CBK were negligible and very small and taken approximately (QY < 0.1%).

3.7. Photo-electrochemical studies

To study the charge transfer at the interfaces between electrode and electrolyte, we carried out electrochemical impedance spectroscopy (EIS) measurments between 100 mHz and 1 MHz at 0 V vs. open circuit potential. Photo-electrochemical studies were performed on materials and compared with analogous commercial titania P25-WT. Nyquist plots (Figure 10) were used to assess the charge transfer resistance (R_{ct}) which scales linearly with the length chord (on the real impedance axis) of the arc of the Nyquist plot in the high to medium frequency region, i.e., where charge transfer control regime is in place.[45] The values obtained from the Nyquist plots are reported in Tables 2 and 3 with respect to open circuit voltage. In the case of hydride reduced samples, whether calcined under H_2 or under inert Ar atmospheres, the coloured samples all showed smaller charge transfer resistance than the starting titania P25-WT, clearly highlighting their greater conductivity and improved charge transfer properties at the solid-electrolyte interface. In general, it can be concluded that all the coloured titania materials will facilitate faster charge transfer at the electrode-electrolyte interface compared to commercial P25-WT; interestingly though, the samples with optimal charge transfer when compared to the starting material are the ones showing the least amount of crystal defects amongst all the coloured samples, i.e., the ones with the paler colour, 458 Ω and 414 Ω for P25-CLB and P25-CBL(A) respectively when compared to 813 Ω of white P25. This suggests that while a controlled amount of crystal defects, such as vacancies and Ti^{3+} centers (as shown in the EPR spectra in Figure 6 and Figure 8 prior to irradiation, since EIS was not conducted under irradiation), can enhance charge transfer properties, an excessive concentration of these defects proves detrimental. This effect was consistently observed in very dark or black samples, which exhibited characteristics approaching those of the original white P25.

3.8. XPS measurements

X-ray photoelectron spectroscopy (XPS) analysis was performed to investigate the chemical states of Ti, O, and Na elements and to correlate with the variation in electronic onset band gap and with EPR studies. In Figure 11 the deconvoluted high-resolution Ti (2p) XP spectra, were fitted using two Gaussian functions superimposed to a tougaard background, for all coloured titania materials and P25-WT. The Figure 11 clearly shows the Ti ($2p_{3/2}$) signals (Ti^{4+}) of coloured titania materials located at binding energy around (458.3-458.5 eV) respectively. These peak positions are the characteristic feature of known phases of TiO_2.[46] We also observed an additional shoulder signal for (Ti^{3+}) located at around (~ 457.4 eV), which is attributed due to the significant amount of intrinsic defects, Ti^{3+} centres present in all coloured materials and significantly fewer in P25-WT. The Ti^{3+} signal gets more strong and intense for blue to black coloured titania, which suggests large number of Ti^{3+} centres formed in black titania (P25-CBK) in a crystal lattice. The results were very consistent with our EPR studies. On another side, the XP spectra in Figure 12 were recorded within the range (1060-1080 eV). The signal positions observed in XP spectra were the characteristics of Na (1s) and Ti (LMM) which overlapped with each other in this region and are well in agreement with literature.[47] Therefore, the XP spectra were deconvoluted and fitted using three Gaussian functions superimposed to a shirley background. The Na (1s) signal in XP

spectra observed at binding energy around (~ 1071.2 eV) gets more and more intense as the prepared material colour changes from (light blue to black) for a series of prepared coloured materials, it suggests more incorporation of Na^+ ion inside the lattice in black titania (P25-CBK) relative to light blue to dark blue titania (P25-CLB, P25-CBL, P25-CBB) prepared under H_2 atmosphere. In contrast, no such signal was observed in commercial titania P25-WT. The other two observed signals in XP spectra were of Ti (LMM) which were centred at binding energy around (~1067.2 eV) and (~1072.2 eV) in all prepared coloured titania as well as in P25-WT.

Auger electron spectroscopy (AES) analysis was also performed, and the AE spectra were recorded for a series of coloured titania prepared via the chemical reduction method under hydrogen atmosphere and commercial titania, P25-WT. It is a very well-known, established technique to get surface chemical composition. The atomic concentration of oxygen and Ti elements were calculated by using the relative peak area with its relative sensitive factors (RSF) from the instrument in the AE spectra plot. The atomic concentration calculation for each oxygen and Ti element was determined using the equation 1.[48,49]

$$\text{Atom}(\%)\ \text{element of X} = [(I_x/S_x)/(\sum I_i/S_i)]\ \text{x}\ 100 \text{.....(1)}$$

where I_x is the peak area; here, we consider the relative peak area of the element calculated using the product of the peak gradient and square of the width, i.e. hw^2 in a differential spectrum (Figure 13). It is suggests to be more accurate way compared to considering peak-to-peak amplitude in the direct energy spectrum.[49] Here, in AE spectra, the Ti (LMM) signal (385.5 eV) was used for the quantification. Similarly, to calculate atomic concentration for oxygen, O (KLL) signal (513 eV) is considered for calculation. Here, it is noteworthy in AE spectra that one of the signal corresponding to Na (KLL) overlapped with Ti (LMV) peak, which clearly gives evidence that the Na element is present in all prepared coloured titania. Further, the relative atomic concentration (O/Ti) ratio was calculated, and values were tabulated in Table 2. The observed relative ratio for (O/Ti) suggests coloured titania are very much oxygen deficient relative to commercial titania, P25-WT. The observed AES result suggests our prepared coloured titania are oxygen deficient relative to P25-WT. These results were very much aligned with our EPR and XPS results.

3.9 FT-Raman studies

The Raman spectroscopy measurements were performed on all coloured titania samples and commercial titania, P25-WT. The Raman bands observed in P25-WT are in good agreement with published data.[50-52] Furthermore, In (Figure S10 ESI†), as expected, higher wavenumber peaks are broader and weaker in the observed Raman spectra of P25-PBL, which indicate a lack of short-range order in -Ti-O-Ti- symmetry on reduction. Here, a clear blue shift was observed at the very first intense peak (Figure S10 (a) (inset), ESI†) for E_g mode from 143.6 cm^{-1} to 150.4 cm^{-1}. The surface pressure broadening was also observed due to localised effects in peaks at high wavenumber, and it clearly indicates the original symmetry of P25-WT was broken down due to the disordered surface, it is also well in agreement with the literature.[53,54] In the case of metal hydride reduced colour titania samples, the blue shift observed in Raman spectra (Figure S11 (a) and (b), ESI†) with the vanishing of the most intense and other peaks, as the colour gets more and more intense (blue to black) with which suggests original -Ti-O-Ti- symmetry were mostly broken at surface and/or either surface get disintegrated, or deteriorated utterly. These results were further in alignment and supported by our TEM studies.

3.10. Photocatalytic hydrogen evolution

The photocatalytic activity of all titania samples was assessed for hydrogen evolution reaction without co-catalyst (Figure 14). The remarkable activity observed for the coloured titania, e.g., P25-PBL, prepared *via* the physical method, was ~ 2.6 times higher (Figure 14a) than the coloured samples (e.g., P25-CBL; ~ 1.5 times; Figure 14b & Figure 14c) prepared via the chemical method, which in turn significantly higher than the corresponding white titania, viz., P25-WT. This could be attributed to the abundant presence of intrinsic defects favouring facile hydrogen generation. That is, the defects observed in the case of coloured titania prepared *via* the physical pressure method are mainly due F-centre, i.e., a vacant oxygen site containing a single electron present which is very much facile and contributes much higher significant photocatalytic hydrogen evolution, whereas coloured samples prepared by chemical pressure method consists of distinct intrinsic defects including vacancy defects and reduced titania, i.e., Ti^{3+} centres, even without any induced irradiation which also shows significant photocatalytic hydrogen evolution relative to P25-WT where only fever intrinsic defects was observed.

A detailed study discussed in the EPR section clearly suggests that after photo-induced UV irradiation, additional signals are observed which are associated with an anisotropic *g*-tensor. In the case of the samples prepared under an argon atmosphere, P25-CBL(A) and P25-CBB(A), both contain very similar paramagnetic species. However, the latter has a slightly larger concentration of surface/subsurface or bulk-reduced Ti^{3+} centres, forming magnèli phases and/or disintegrated titania. Similar results are expected for samples prepared *via* the chemical reduced method under a hydrogen atmosphere. These results were well aligned with other spectroscopic analyses, as evidenced from XRD, XPS and AES studies. The lower R_{ct} values obtained for coloured titania samples relative to white titania from photo-electrochemical measurements further support the photocatalytic activity results. Our EPR results were much aligned with the literature reports.[39,40] EPR signal for P25-PBL observed at $g = g_e = 2.002$ attributed to an F-centre, interestingly do not show any evidence of trapped holes or Ti^{3+} centres. Although in literature,[55] pristine titania treated under vacuum or hydrogen reduction conditions get EPR signal at $g = 1.96$ due to the formation of Ti^{3+} centres. Therefore, it can clearly be understood from structural imperfection in TiO_2,

i.e., specific intrinsic defects (F-centre) are much more essential to get significantly higher solar hydrogen generation.

4. Conclusions

In summary, defect-induced colored titania was successfully synthesized using both physical and chemical methods under controlled conditions, with comprehensive material characterization conducted to elucidate the formation of intrinsic defects. Distinct defect types were identified depending on the synthesis method. The colored material P25-PBL, prepared *via* the physical method, exhibited a significant presence of polarized electrons, while the chemical synthesis predominantly generated Ti^{3+} centers within the surface/subsurface and bulk lattice. Surface/subsurface F-centers, crucial for enhanced photoactivity, play a key role in facilitating the transfer of conduction electrons from the semiconductor surface to reduce hydrogen ions into hydrogen molecule. Consequently, the photocatalytic hydrogen evolution rate observed for the physical method was about 1.75 times higher than that achieved *via* the chemical method. Both methods produced materials with performance significantly superior to the benchmark commercial white titania, P25-WT. Our findings from XRD, EPR, PL, TEM, XPS, AES, and Raman analyses were consistent and aligned with previous reports. This study concludes that free electrons are more critical than Ti^{3+} centers for solar hydrogen production. Among all catalysts studied, P25-PBL demonstrated the highest photocatalytic hydrogen evolution, achieving an average rate of 0.78 mmol g^{-1} h^{-1} over a five-hour reaction period without the use of a cocatalyst, which is approximately 2.6 times higher than that of commercial titania P25-WT (0.30 mmol g^{-1} h^{-1}).

Conflicts of interest

"There are no conflicts to declare".

Acknowledgements

The authors thank Department of Science and Technology (DST), New Delhi, for funding NCCR, IIT-Madras; Professor Lynn F. Gladden and Professor Mick D. Mantle for the encouragement and support. This work is partially supported by the grant-in-aid for scientific research on priority areas under technology systems development (TSD) programme on priority areas - Generation of Solar Hydrogen (DST/TSG/SH/2011/106-G). PS and HM gratefully acknowledge Queen's University Belfast for providing the agility grant.

References

1 A. Fujishima and K. Honda, *Nature*, 1972, **238**, 37–38.
2 X. Chen and S. S. Mao, *Chem. Rev.*, 2007, **107**, 2891–2959.
3 A. Kudo and Y. Miseki*, Chem. Soc. Rev*., 2009, **38**, 253–278.
4 H. P. Maruska and A. K. Ghosh, *Sol. Energy Mater*., 1979, **1**, 237–247.
5 D, Lawless, PhD Thesis, Concordia University, 1993.
6 S. Sato, Chem. *Phys. Lett*., 1986, **123**, 126-128.
7 R. Asahi, T. Morikawa, T. Ohwaki, K. Aoki and Y. Taga, *Science*, 2001, **293**, 269–271
8 W. Choi, A. Termin and M. R. Hoffmann, *J. Phy. Chem*., 1994, **98**, 13669–13679.
9 Z. Zhang, Q. Wu, G. Johnson, Y. Ye, X. Li, N. Li, M. Cui, J. D. Lee, C. Liu, S. Zhao, S. Li, A. Orlov, C. B. Murray, X. Zhang, T. B. Gunnoe, D. Su and S. Zhang. *J. Am, Chem. Soc*., 2019, **141**, 16548–16552.
10 M. J. Yang, C. Hume, S. Lee, Y-H. Son and J. -K. Lee, *J. Phys. Chem. C*, 2010, **114**, 15292–15297.
11 Y-F Li, D. Xu, J. Oh, W. Shen, X. Li and Y. Yu, *ACS Catal.*, 2012, **2**, 391–398.
12 J.W. Liu, R. Han, Y. Zhao, H. T. Wang, W. J. Lu, T. F. Yu and Y. X. Zhang, *J. Phys. Chem. C*, 2011, **115**, 4507–4515.
13 X. Chen, L. Liu, P.Y. Yu and S.S. Mao, *Science*, 2011, **331,** 746–750.
14 S. Tominaka, Y. Tsujmoto, Y. Matsushita and K. Yamaura, *Angew. Chem. Int. Ed*., 2011, **50**, 7418–7421.
15 S. Tominaka, *Chem. Commun*., 2012, **48**, 7949-7951.
16 M.A. Hayward, M. A. Green, M.J. Rosseinsky, J. Sloan, *J. Am. Chem. Soc*., 1999, **121**, 8843–8854.
17 A. Naldoni, M. Allieta, S. Santangelo, M. Marelli, F. Fabbri, S. Cappeli, C. L. Bianchi, R. Psar and V. D. Santo, *J. Am. Chem. Soc.*, 2012, **134**, 7600–7603.
18 S. Kalathil, M. M. Khan, S. A. Ansari, J. Lee and M. H. Cho, *Nanoscale*, 2013, **5**, 6323–6326.
19 H. Lu, B. Zhao, R. Pan, j. Yao, J. Qiu, L. Luo and Y. Liu, *RSC Adv*., 2014, **4**, 1128–1132.
20 H. Tan, Z. Zhao, M. Niu, C. Mao, D. Cao, D. Cheng, P. Feng and Z. Sun, *Nanoscale*, 2014, **6**, 10216–10223.
21 M. Ye, J. Jia, Z. Wu, C. Qian, R. Chen, P. G. O'Brien, W. Sun, Y. Dong and G. A. Ozin, *Adv. Energy Mater*., 2017, **7**, 1601811.
22 Y. Liu, H. Feng, X. Yan, J. Wang, H. Yang, Y. Du and W. Hao, *Dalton Trans*., 2017, **46**, 10694–10699.
23 D. Ariyanti, L. Mills, J. Dong, Y. Yao and W. Gao, *Mater. Chem. Phys.*, 2017, **199**, 571–576.
24 X. Chen, L. Liu and F. Huang, *Chem. Soc. Rev*., **44**, 2015, 1861-1885.
25 P. Selvam, S. Gupta, Pat. IN398100, 2020.
26 S. Gupta and P. Selvam, *2nd National Conference on Materials For Energy Conversion and Storage*, Puducherry, 2016, p.111.
27 P. Selvam and S. Gupta, *World Hydrogen Energy Conference,* Zaragoza, 2016, p.29.
28 R. K. Sankarnarayan, S. Gupta and P. Selvam, "*3rd International Conference on Nanomaterials*", Australia, 2018, p.40.
29 S. Gupta and P. Selvam, *3rd International Conference of Advanced Energy Materials*, England, 2018, p.194.
30 S. K. Vatti, S. Gupta, R. P. Raj and P. Selvam, *New J. Chem*., 2020, **44**, 16269–16284.
31 B. Ohtani, O. O. Prieto-Mahaney, D. Li and R. Abe, *J. Photochem. Photobiol., A*, 2010, **216**, 179–182.
32 M. Ye, J. Jia, Z. Wu, C. Qian, R. Chen, P. G. O'Brien, W. Sun, Y. Dong and G. A. Ozin, *Adv. Energy Mater.*, 2017, **7**, 1601811
33 P. Kubelka and F. Munk, *Z. Tech. Phys.,* 1931, **12**, 593–601.
34 H. G. Hecht, *J. Res. NBS A Phys. Ch*., 1976, **80**, 567.
35 J. Tauc, R. Grigorovici, A. Vancu, *Phys. Stats. Sol.,* 1966, **15**, 627–637.

36 B. D. Cullity and S.R. Stock, *Elements of X-ray Diffraction*, Printice-Hall, New Jersey, 3rd edn, 2001.

37 K. S. W. Sing, *Pure Appl. Chem.*, 1982, **54**, 2201–2218.

38 C. P. Kumar, N. O. Gopal, T. C. Wang, M. S. Wong and S. C. Ke, *J. Phys. Chem. B*, 2006, **110**, 5223–5229.

39 R. F. Howe and M. Grätzel, *J. Phys. Chem*., 1985, **89**, 4495–4499.

40 S. Misra, S. Andronenko, D. Tipikin, J. Freed, V. Somani and O. Prakash, J. Magn. Magn. Mater., 2016, **401**, 495–505.

41 J. Yu, L. Qi and M. Jaroniee, *J. Phys. Chem*. *C*, 2010, **114**, 13118–13125.

42 Z. Wang, C. Yang, T. Lin, H. Yin, P. Chen, D. Wan, F. Xu, F. Huang, J. Lin, X. Xie and M. Jiang, *Adv. Funct. Mater*., 2013, **23**, 5444–5450.

43 M. Saif, S. M. K. Aboul-Fotouh, S. A.EI-Molla, M. M. Ibrahim and L. F. M. Ismail, *Spectrochimi. Acta, Part A*., 2014, **128**, 153–162.

44 S. Mathew, A. K. Prasad, T. Benoy, P. P. Rakesh, M. Hari, T. M. Libish, P. Radhakrishnan, V. P. N. Nampoori and C. P. G. Vallabhan, *Journal of Fluorescence*, 2012, **22**, 1563–1569.

45 Y. Yang, X, Ji, M, Jing, H. Hou, Y, Zhu, L. Fang, X. Yang, Q. Chen and C.E. Banks, *J. Mater. Chem. A*, 2015, **3**, 5648–5655.

46 R. Sanjines, H.Tang, F. Berger, F. Gozzo, G. Margaritonto and F. Levy, *J. Appl. Phys*., 1994, **75**, 2945–2951.

47 S-E Kim, J-G Lee, L. Ling, S. E. Liu, H-K Lim, V. K. Sangwan, M.C. Hersam and H-S Lee, *Adv. Mater*., 2022, **34**, 2106913.

48 C. D. Wagner, L. E. Davis, M. V. Zeller, J. A. Taylor, R. M. Raymond and L. H. Gale, *Surf. Interface Anal*., 1981, **3**, 211.

49 M. P. Seah, *Surf. Interface Anal*., 1979, **1**, 86–90.

50 T. Ohsaka, F. Izumi and Y. Fujiki, *J. Raman Spectrosc*., 1978, **7**, 321–324.

51 M. Ben Yahia, F. Lemoigno, T. Beuvier, J.-S. Filhol, M. Richard-Plouet, L. Brohan and M.-L. Doublet, *J. Chem. Phys., 2009*, **130**, 204501.

52 T. Beuvier, M. Richard-Plouet and L. Brohan, *J. Phys. Chem. C*, 2009, **113**, 13703–13706.

53 S. K. Gupta, R. Desai, P. K. Jha, S. Sahoo and D. Kirin, *J. Raman Spectrosc.*, 2010**, 41**, 350–355.

54 A. Turkovic, M. Ivanda, A. Drasner, V. Vranesa and M. Persin, *Thin Solid Films*, 1991, **198**, 199–205.

55 R. D. Iyengar and M. Codell, *Adv. Colloid Interface Sci*., 1972, **3**, 365–388.

Table 1. Structural, electronic, textural parameters and photocatalytic hydrogen evolution characteristics of white and coloured titania (physical method) prepared under hydrogen atmosphere.

Catalyst	Structural parameters				[a]τ (nm)	[b]S_{BET} (m^2g^{-1})	[c]Band gap energy (eV)		[d]r_{H_2} ($\mu mol\ g^{-1}h^{-1}$)
	Anatase		*Rutile*						
	wt %	Lattice constant (Å)	wt %	Lattice constant (Å)			Abs.	$[F(R)–E]^{1/2}$	
P25-WT	84.5	$a = 3.79104(4)$ $c = 9.5207(2)$ $V = 136.832(4)$ Å^3	15.5	$a = 4.60093(12)$ $c = 2.96312(14)$ $V = 62.725(4)$ Å^3	22 (A) 38 (R)	45	3.12	3.21	300
P25-PBL	82.0	$a = 3.79322(4)$ $c = 9.5259(2)$ $V = 137.063(4)$ Å^3	18.0	$a = 4.6040(8)$ $c = 2.9651(9)$ $V = 62.85\ (3)$ Å^3	29 (A) 44 (R)	30	3.00	3.03	780

[a]Crystallite size from XRD; [b]Surface area; [c]Energy band gap; [d]Rate of hydrogen evolution.

Table 2. Structural, electronic, textural parameters, electrochemical data and photocatalytic hydrogen evolution characteristics of white and coloured titania (chemical method) under hydrogen atmosphere.

Catalyst	Structural parameters				[a]τ (nm)	[b]S_{BET} (m^2g^{-1})	[c]Band gap energy (eV)		[d]R_{ct} (Ω)	AES (O/Ti ratio)	[e]r_{H_2} ($\mu mol\ g^{-1}h^{-1}$)
	Anatase		*Rutile*								
	wt %	Lattice constant (Å)	wt %	Lattice constant (Å)			Abs.	$[F(R)–E]^{1/2}$			
P25-WT	84.5	$a = 3.79104(4)$ $c = 9.5207(2)$ $V = 136.832(4)$ Å^3	15.5	$a = 4.60093(12)$ $c = 2.96312(14)$ $V = 62.725(4)$ Å^3	22 (A) 38 (R)	45	3.12	3.21	813	2.08	300
P25-CLB	83.8	$a = 3.79162(8)$ $c = 9.5206(2)$ $V = 136.872(8)$ Å^3	16.2	$a = 4.60205(15)$ $c = 2.96308(14)$ $V = 62.754(6)$ Å^3	20 (A) 31 (R)	45	2.94	2.95	458	1.94	360
P25-CBL	83.4	$a = 3.79197(9)$ $c = 9.5205(3)$ $V = 136.883(6)$ Å^3	16.6	$a = 4.60237(18)$ $c = 2.96302(18)$ $V = 62.762(5)$ Å^3	20 (A) 30 (R)	45	….	….	537	1.91	440
P25-CBB	83.2	$a = 3.7947(2)$ $c = 9.5167(7)$ $V = 137.038(17)$ Å^3	16.8	$a = 4.6128(5)$ $c = 2.9605(5)$ $V = 62.990(14)$ Å^3	17 (A) 23 (R)	46	….	….	618	1.88	460
P25-CBK[f]	81.1	$a = 3.7988(5)$ $c = 9.4928(15)$ $V = 137.05(4)$ Å^3	18.9	$a = 4.6305(15)$ $c = 2.9526(11)$ $V = 63.30(4)$ Å^3	11 (A) 20 (R)	48	….	….	688	1.82	330

[a]Crystallite size from XRD; [b]Surface area; [c]Energy band gap; [d]Charge transfer resistance; [e]Rate of hydrogen evolution; [f]Including Magnéli phase.

Table 3. Structural, electronic, textural parameters, electrochemical data and photocatalytic hydrogen evolution characteristics of white and coloured titania (chemical method) prepared under argon atmosphere.

Catalyst	Structural parameters									
	Anatase		*Rutile*		[a] τ	[b] S_{BET}	[c] Band gap energy *(eV)*		[d] R_{ct}	[e] r_{H_2}
	wt %	Lattice constant (Å)	wt %	Lattice constant (Å)	*(nm)*	(m^2g^{-1})	Abs.	$[F(R)–E]^{1/2}$	*(Ω)*	$(\mu mol\ g^{-1}h^{-1})$
P25-WT	84.5	$a = 3.79104(4)$ $c = 9.5207(2)$ $V = 136.832(4)$ Å^3	15.5	$a = 4.60093(12)$ $c = 2.96312(14)$ $V = 62.725(4)$ Å^3	22 (A) 38 (R)	45	3.20	3.21	813	300
P25-CBL(A)	84.3	$a = 3.79216(6)$ $c = 9.5218(2)$ $V = 136.928(4)$ Å^3	15.7	$a = 4.60226(14)$ $c = 2.96350(15)$ $V = 62.769(4)$ Å^3	21 (A) 34 (R)	50	2.97	2.99	414	450
P25-CBB(A) [f]	79.4	$a = 3.7898(2)$ $c = 9.5056(9)$ $V = 136.524(19)$ Å^3	20.6	$a = 4.6024(10)$ $c = 2.9629(11)$ $V = 62.76\ (3)$ Å^3	19 (A) 26 (R)	52	….	….	664	380

[a]Crystallite size from XRD; [b]Surface area; [c]Energy band gap; [d]Charge transfer resistance; [e]Rate of H_2 evolution; [f]Including Magnéli phase

Table 4. Spin Hamiltonian parameters of the paramagnetic species detected in P25-CBL(A).

Signal	Paramagnetic species	g_1	g_2	g_3
A	Vacancy	2.008	2.003	2.001
B	Surface Ti^{3+} in anatase TiO_2	1.980	1.980	1.957
C	Surface Ti^{3+} in rutile TiO_2	1.969	1.969	1.947
D	Ti^{4+}–$O^{\bullet-}$–Ti^{4+}–OH^- in anatase	2.015	2.008	2.002
E	Ti^{4+}–O_2^- in anatase	2.022	2.0115	2.003

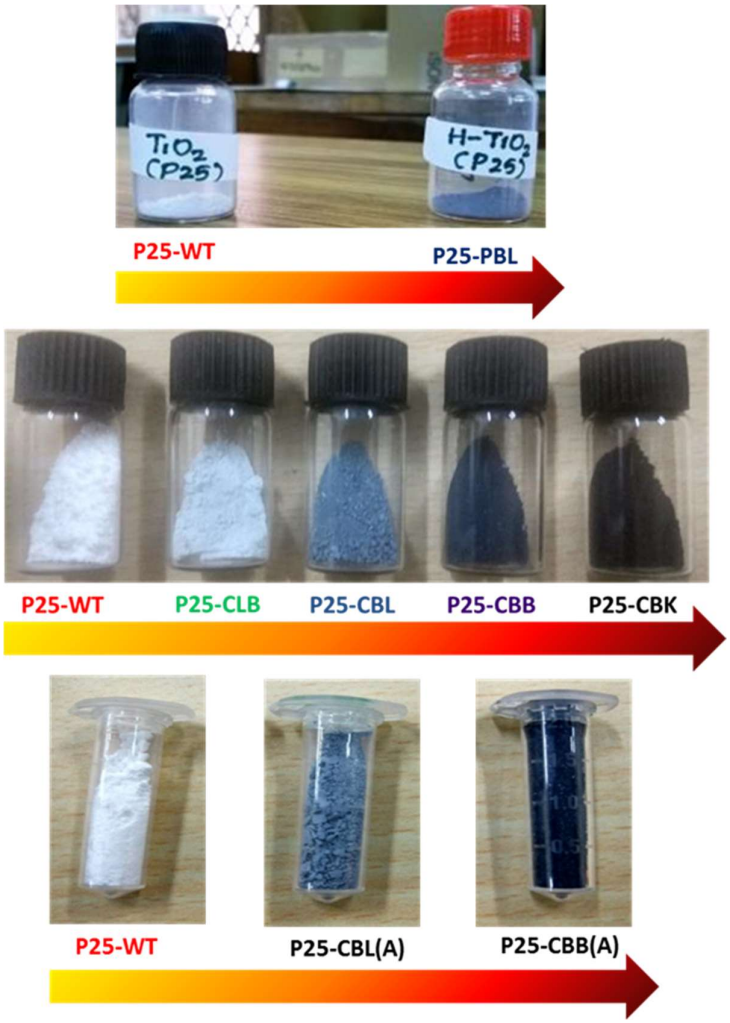

Figure 1. Pictorial representation of commercial white P25-WT and series of coloured titania prepared by physical and chemical method.

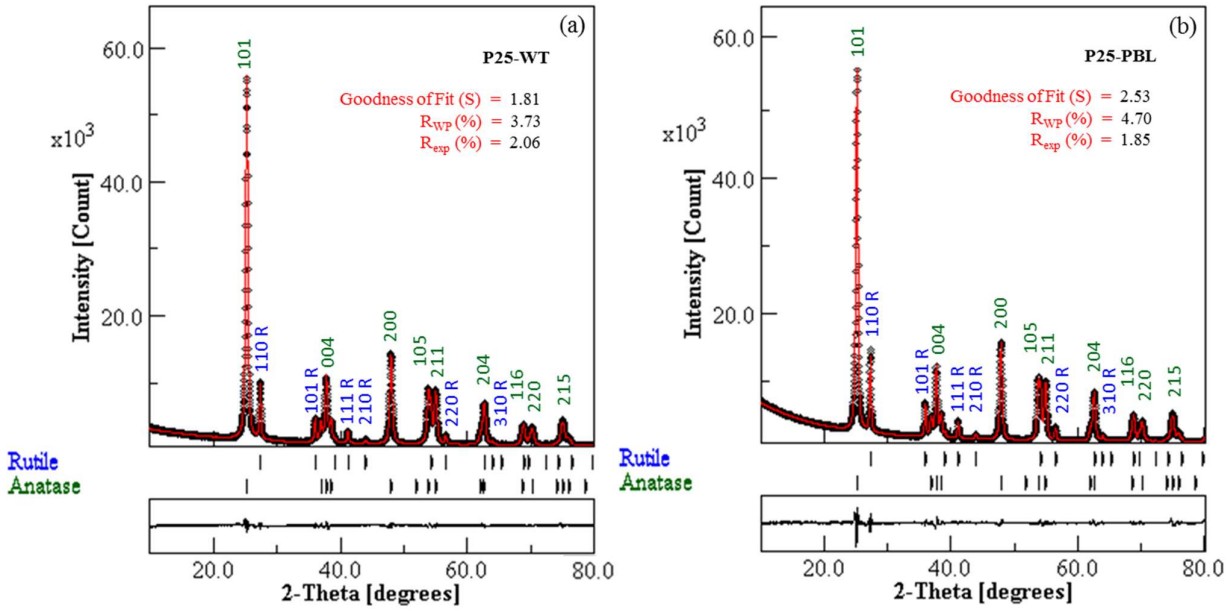

Figure 2. Rietveld refined Powder XRD patterns of coloured titania prepared *via* physical method: (a) P25-WT and (b) P25-PBL.

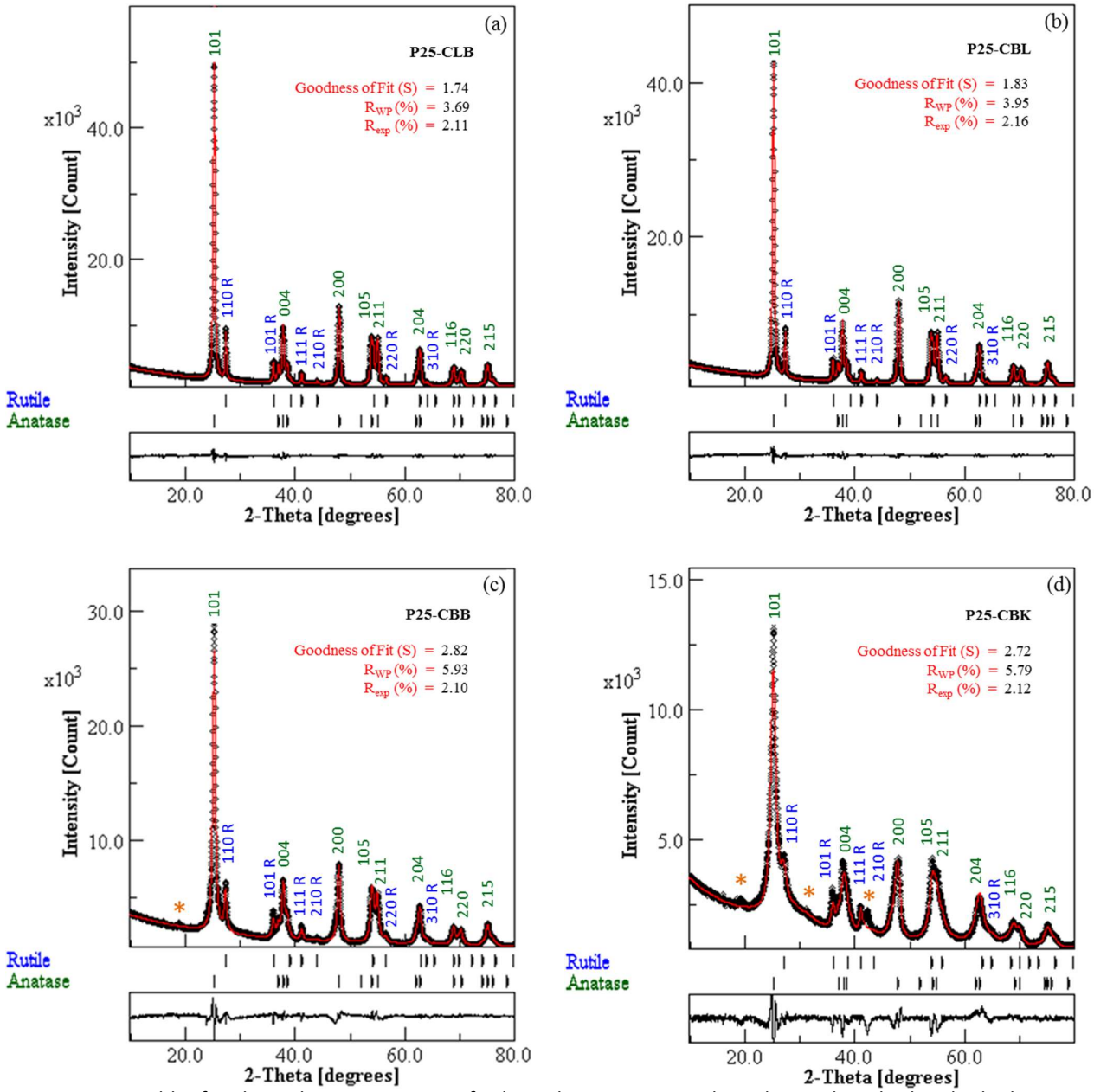

Figure 3. Rietveld refined Powder XRD patterns of coloured titania prepared *via* chemical method under hydrogen atmosphere (a) P25-CLB; (b) P25-CBL; (c) P25-CBB and (d) P25-CBK.

Figure 4. Powder XRD patterns of white and blue titania.

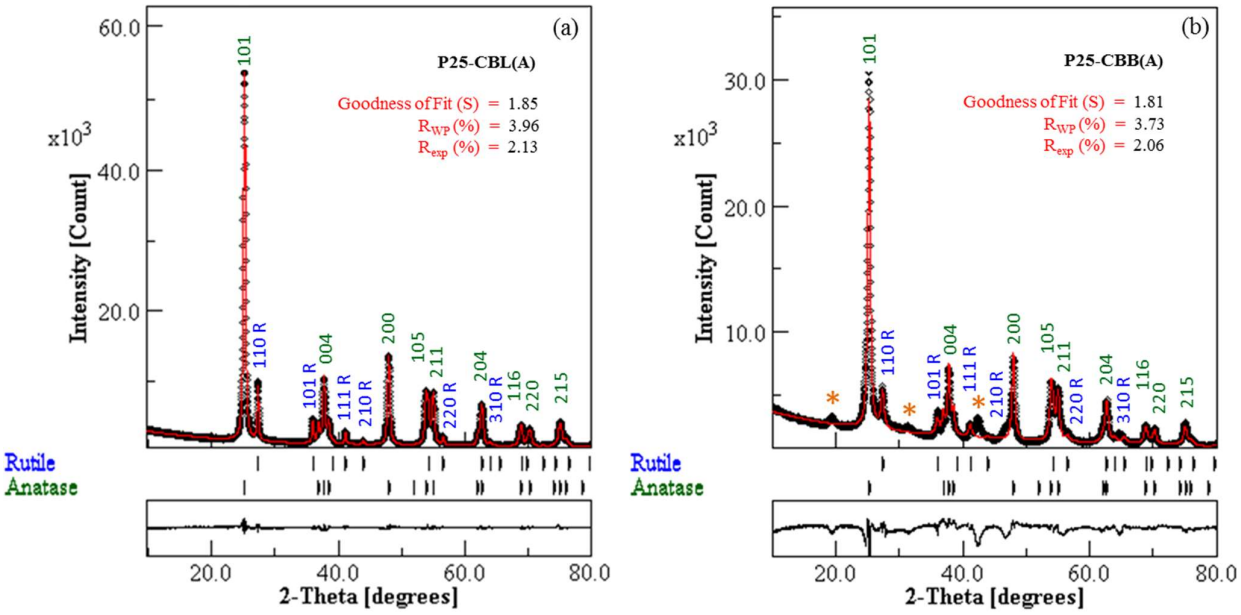

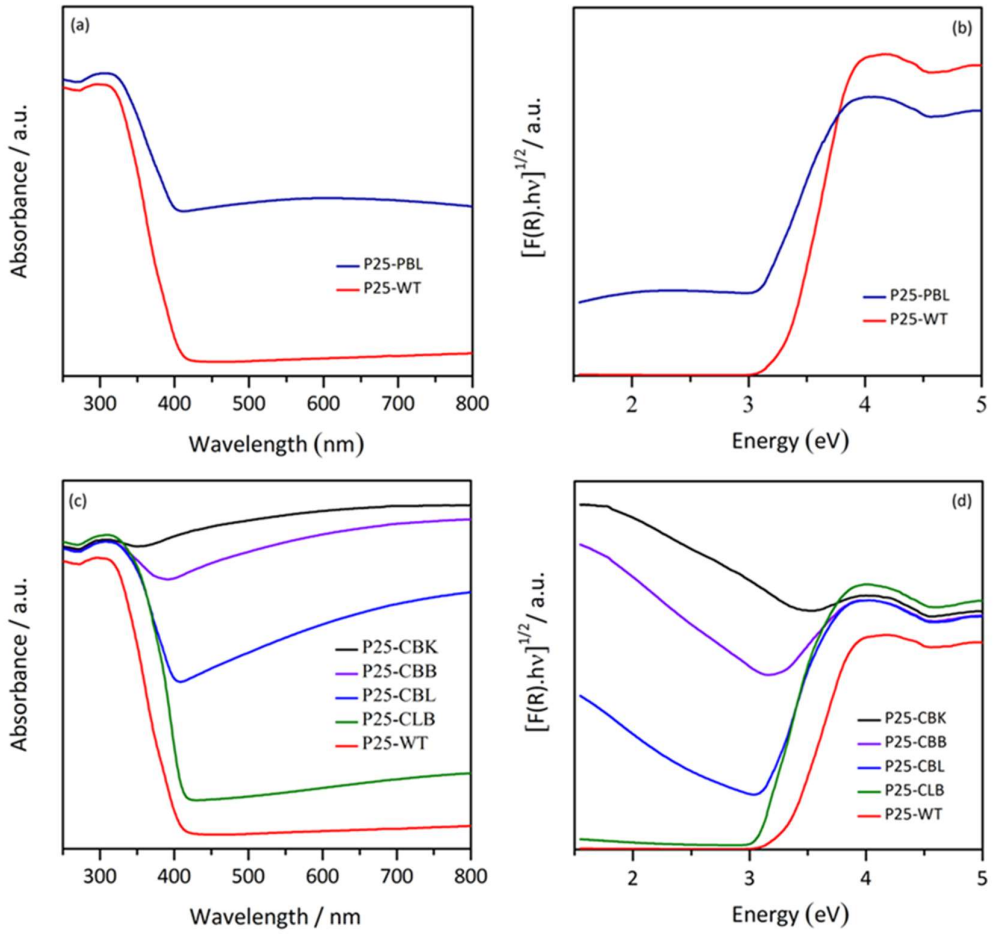

Figure 4. DRUV-visible absorbance spectra plot (a) and (c) ; Kubelka-Munk plot (b) and (d) of various prepared coloured titania and P25-WT.

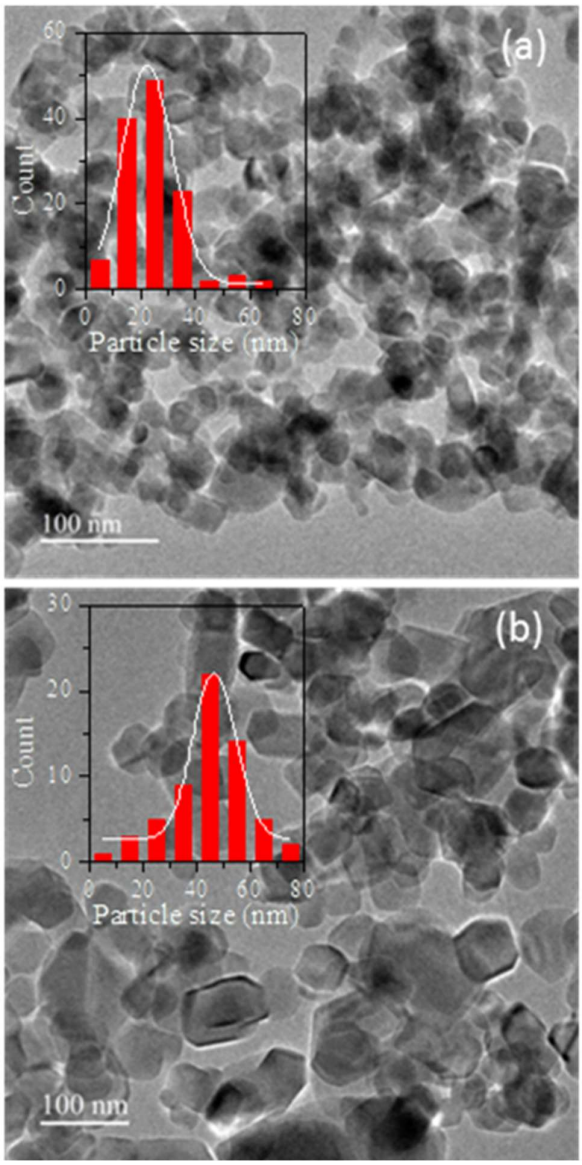

Figure 5. TEM images of (a) P25-WT and (b) P25-PBL with (inset) particle size distribution.

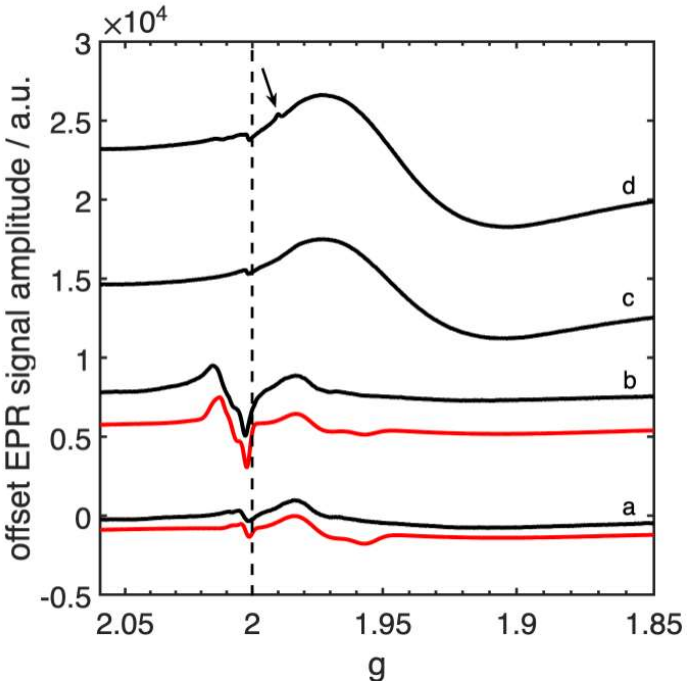

Figure 6. X band CW EPR experimental (black) and simulated (red) spectra of (a) P25-CBL(A) before irradiation; (b) P25-CBL(A) under UV-A irradiation; (c) P25-CBB(A) before irradiation; (d) under UV-A irradiation. Spectra were measured at 77 K.

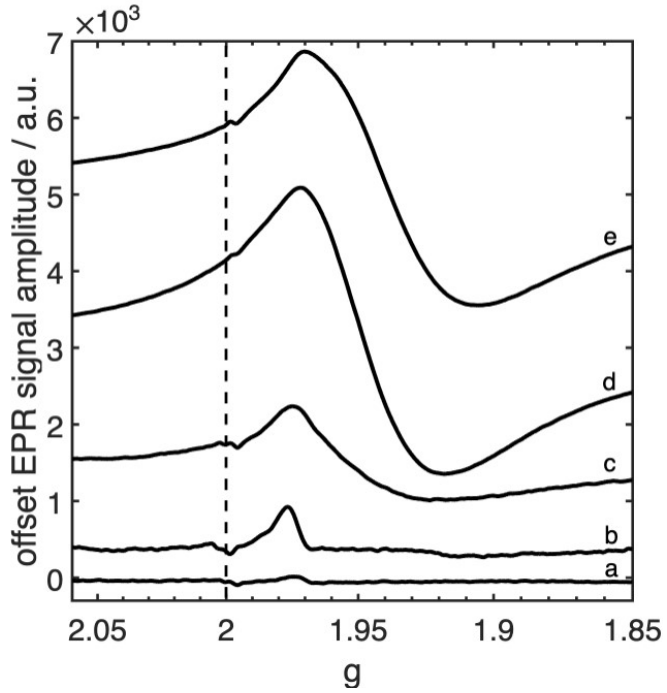

Figure 7. X band CW EPR experimental spectra of (a) untreated white P25; (b) P25-CLB; (c) P25-CBL; (d) P25-CBB; (e) P25-CBK. Spectra were measured at 77 K with no irradiation.

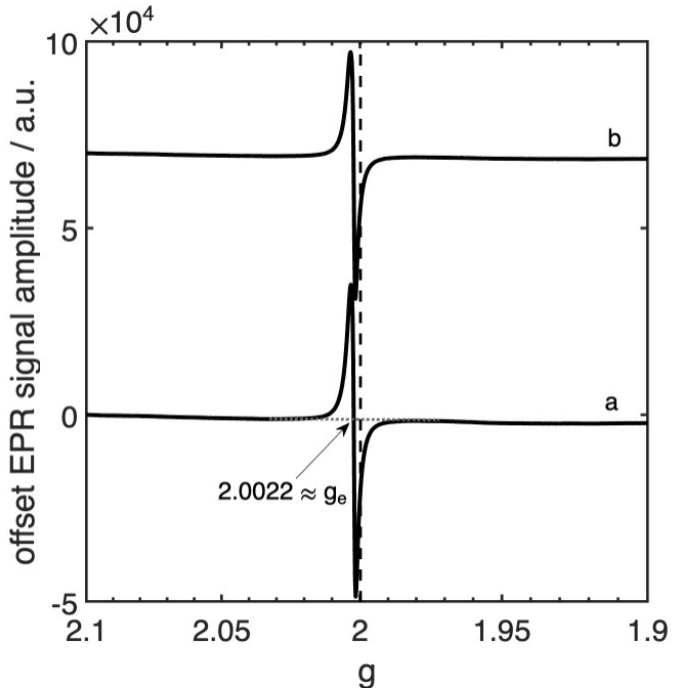

Figure 8. X band CW EPR experimental spectra of (a) P25-PBL before irradiation; (b) P25-PBL under UV-A irradiation. Spectra were measured at 77 K.

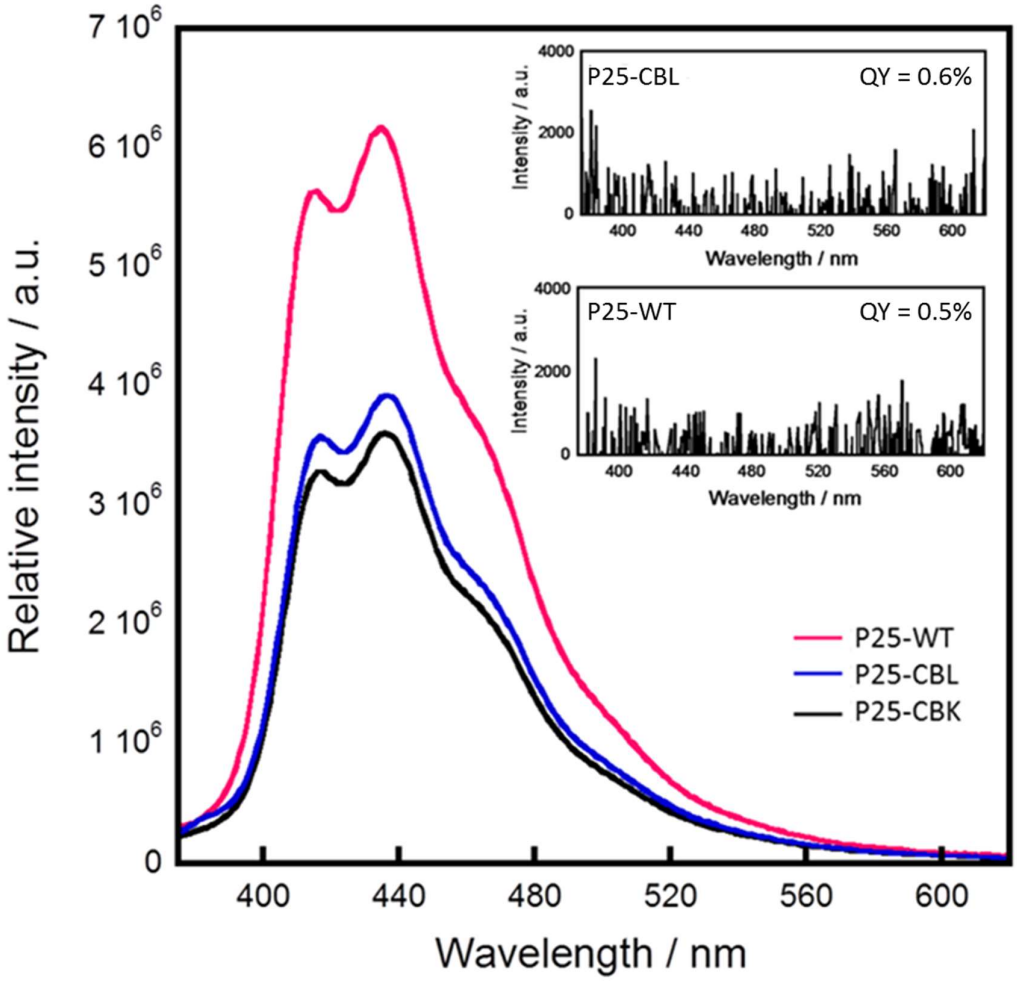

Figure 9. Photoluminescence spectra and quantum yield (inset) of coloured titania (P25-CBL) and commercial titania P25-WT.

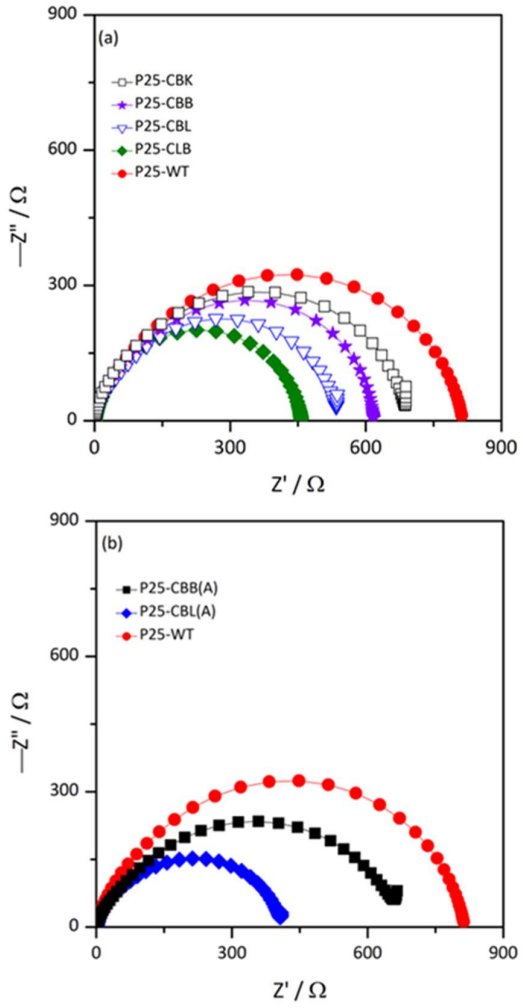

Figure 10. Nyquist plot of P25-WT and coloured titania prepared *via* chemical method under (a) Hydrogen and (b) Argon atmosphere.

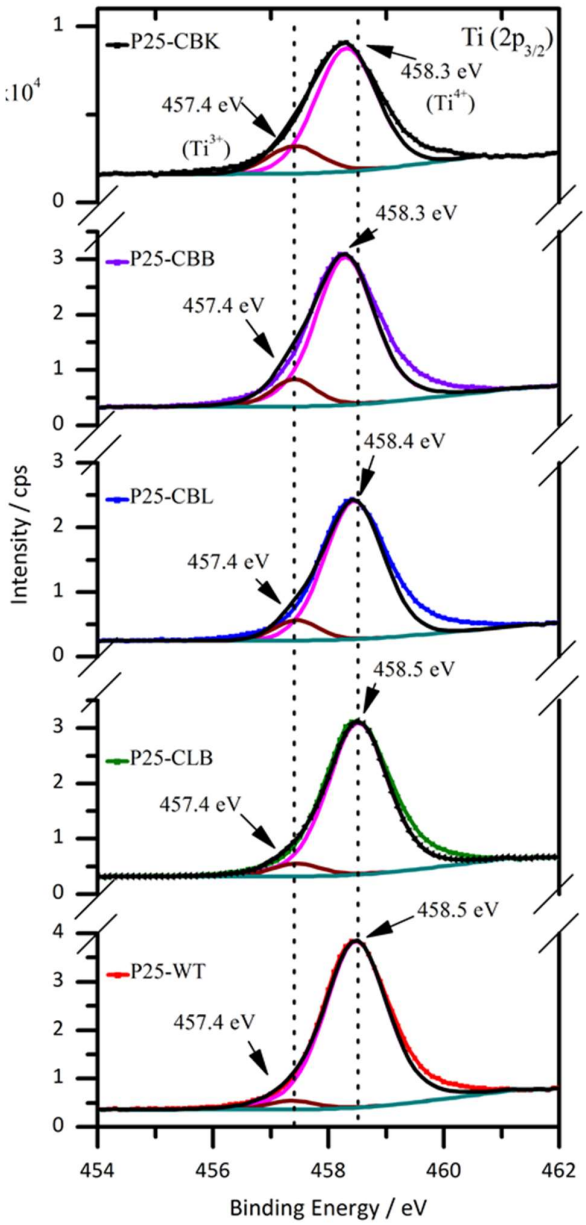

Figure 11. Ti (2p) XP spectra of P25-WT and coloured titania prepared via chemical reduction method in hydrogen atmosphere.

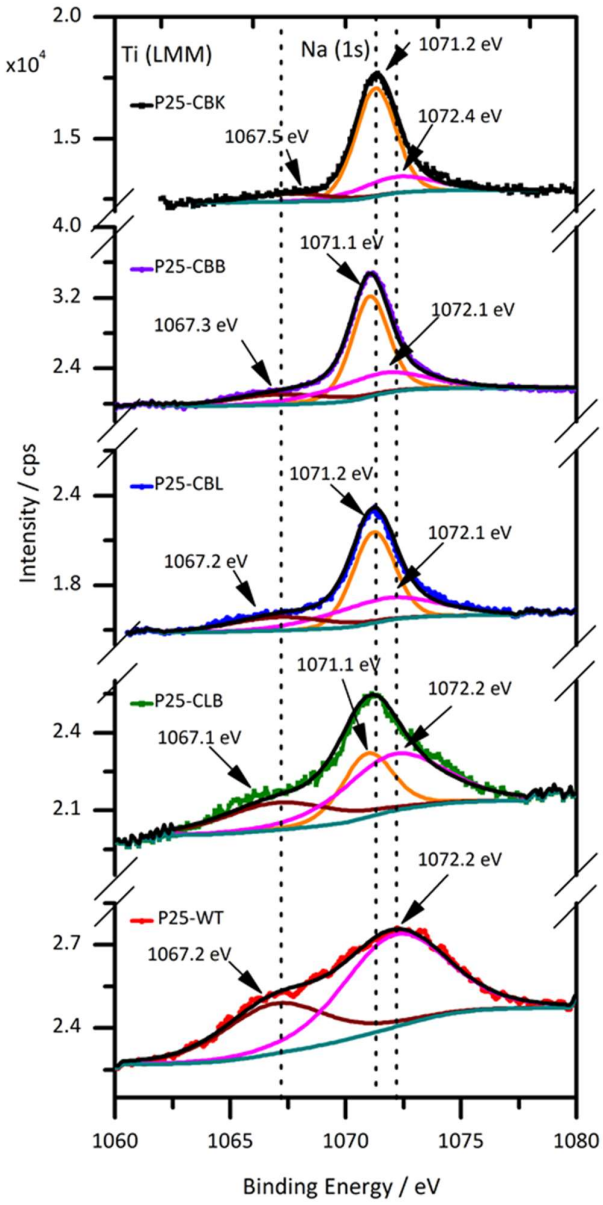

Figure 12. Na (1s) and Ti (LMM) XP spectra of P25-WT and coloured titania prepared via chemical method under hydrogen atmosphere.

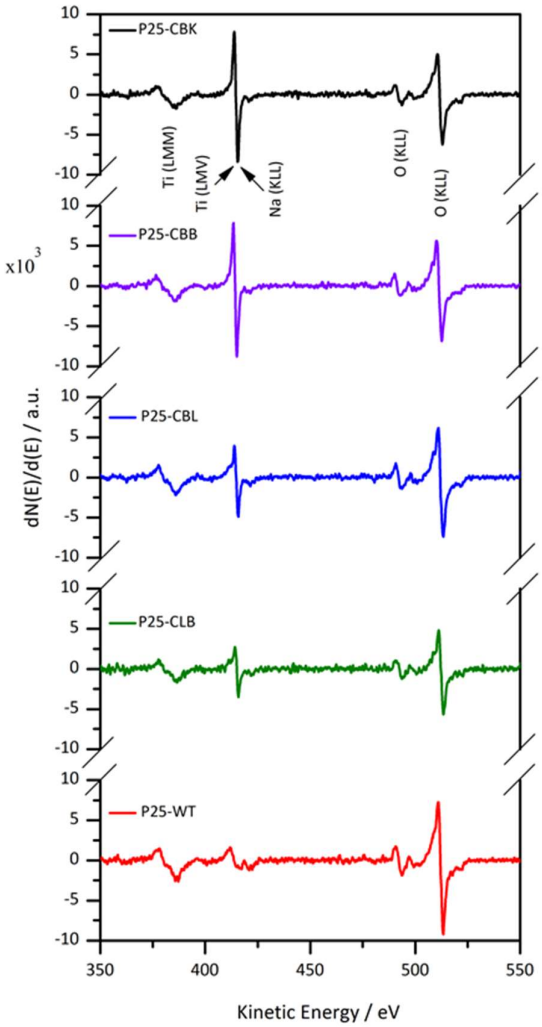

Figure 13. AE spectra of P25-WT and coloured titania prepared via chemical reduction method under hydrogen atmosphere.

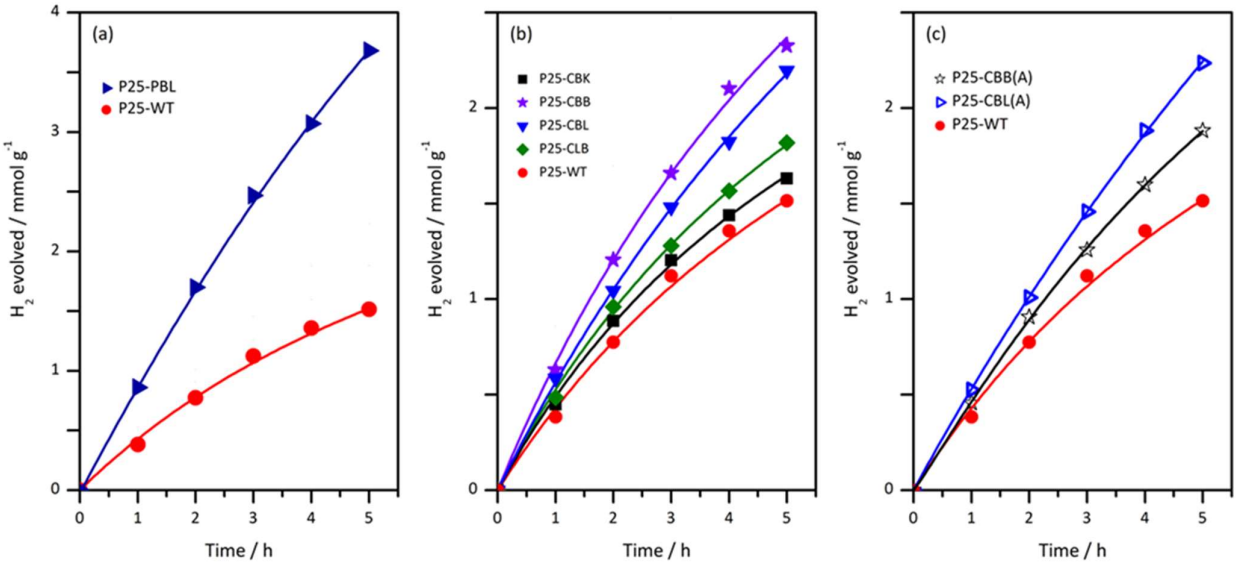

Figure 14. Photocatalytic hydrogen evolution data over coloured titania and P25-WT.